

Quantitative Magnetic Resonance First-Pass Perfusion Analysis: Inter- and Intraobserver Agreement

Olaf M. Mühling,¹ Matthew E. Dickson,¹
Andrey Zenovich,¹ Yimei Huang,¹ Betsy V. Wilson,²
Robert F. Wilson,² Inderjit S. Anand,³ Ravi Teja Seethamraju,¹
Michael Jerosch-Herold,¹ and Norbert M. Wilke¹

¹Department of Radiology, MR-Core Laboratory, Center of Magnetic Resonance Research, and ²Division of Cardiology, Department of Medicine, University of Minnesota Medical School, Minneapolis, Minnesota

³VA Medical Center, Minneapolis, Minnesota

ABSTRACT

Magnetic resonance first-pass (MRFP) imaging awaits longitudinal clinical trials for quantification of myocardial perfusion. The purpose of this study was to assess inter- and intraobserver agreement of this method. Seventeen MRFP studies (14 rest and 3 under adenosine-induced hyperemia) from 14 patients were acquired. Two observers visually graded study quality. Each study was subdivided into eight regions. Both observers analyzed all 17 studies ($8 \times 17 = 136$ regions) for interobserver agreement. Each observer then analyzed 10 of the 17 studies a second time ($2 \times 8 \times 10 = 160$ regions) for intraobserver agreement. Signal intensity curves were obtained with Argus software (Siemens, Iselin, NJ). The maximum amplitude of the impulse response function (R_{max}) and the change of signal intensity (ΔSI_{max}) of the contrast bolus were determined. Intraclass correlation coefficient was used to determine intra- and interobserver agreement. The quality was good or excellent in 14 studies. Intraobserver agreement of R_{max} and ΔSI_{max} were good (0.85 and 0.80,

Address correspondence and reprint requests to Norbert Wilke.

This paper was presented at the Annual Meeting of the International Society of Magnetic Resonance Imaging, Denver, Colo., April 2000.

$n = 160$). Interobserver agreement of R_{max} was fair (0.55, $n = 136$) but improved after exclusion of poor-quality studies (0.88, $n = 112$). Interobserver agreement of ΔSI_{max} was good (0.73) and improved less than R_{max} with study quality (0.83). Interobserver agreement for R_{max} in individual myocardial regions before and after exclusion of studies with poor quality changed most markedly in lateral and posterior regions (0.69 and 0.65 vs. 0.97 and 0.94), where signal-to-noise ratios were reduced compared with anteroseptal regions ($p < 0.01$). Analysis of MRFP images provides good intraobserver agreement. Interobserver agreement of the quantitative perfusion analysis is good under the premise of good image quality.

Key Words: Image analysis; Interobserver agreement; Ischemic heart disease; Perfusion imaging; Signal-to-noise ratio

INTRODUCTION

In regard to newly developed therapeutic revascularization methods, an accurate and clinically applicable noninvasive method for quantification of myocardial blood flow is required. The invasive nature of coronary angiography and the limited spatial resolution of nuclear imaging make these methods appear less eligible for repeated assessment of often mild changes in myocardial perfusion. Magnetic resonance first-pass (MRFP) imaging has recently been validated as a versatile noninvasive clinical tool to quantify myocardial blood flow (1) and to assess collateral flow (2) and angiogenesis (3).

Both the analysis of MR perfusion studies and myocardial blood flow quantification rely on dedicated cardiac perfusion analysis software and model-constrained deconvolution (4,5). Despite the introduction of quantitative perfusion modeling (1,4), image analysis depends on operator interaction and subjective assessment of myocardial perfusion images. The reliability of this quantitative perfusion analysis is unknown. Knowledge about the reliability of the data analysis would be important in regard to longitudinal clinical trials using MRFP perfusion imaging.

In the present study, inter- and intraobserver agreement were determined by repeated analysis of MR perfusion studies from patients with a variety of cardiac pathologies. Additionally, the impact of image quality on intra- and interobserver agreement was assessed.

MATERIALS AND METHODS

Patients

A person not further involved in the study selected randomly 17 nonconsecutive MRFP imaging studies of 14 patients (10 men and 4 women; mean age, 62 ± 10 years; range, 41–77 years). These patients, together with other patients, were enrolled in clinical studies for which

they were referred to our institution between January and August 1999. Myocardial perfusion was assessed in nine patients with single or multivessel coronary artery disease (four patients with previous bypass surgery), in three patients with microvascular dysfunction (coronary Doppler flow reserve = 2.5), and in two patients with nonischemic cardiomyopathy. Table 1 shows baseline hemodynamic data and body mass index. In all patients, their diagnosis was established by conventional tests (left heart catheter, coronary angiogram, intracoronary Doppler-flow measurement; $n = 3$). At the time of the study, all patients were in stable clinical conditions without signs of heart failure or acute myocardial ischemia. Informed consent was acquired for all participants, in accordance with the requirements of the Institutional Review Board for Protection of Human Subjects at the University of Minnesota.

Image Acquisition

Quantitative imaging was performed on a commercially available 1.5-T whole body system (VISION, Siemens Medical Systems, Erlangen, Germany) using a

Table 1
Ejection Fraction (EF), Heart Rate (HR), and Body Mass Index (BMI) of the Study Population

	EF (%)	HR (1/min)	BMI*
Whole study population*	54.5 ± 9.8	59 ± 9.0	29.9 ± 6.5
Study population with:			
EF < 50% ($n = 4$)			46.3 ± 3.1
EF > 50% ($n = 10$)			62.8 ± 5.9
BMI > 30 ($n = 3$)			36.8 ± 3.7
BMI 25–30 ($n = 6$)			27.8 ± 0.6
BMI < 25 ($n = 5$)			22.6 ± 3.1

*Values are means \pm SD.



four-channel phased-array body coil. Multislice imaging with four slices in a double-oblique short-axis orientation was performed using a snapshot-fast low angle single shot sequence with linear k-space ordering. The in-plane resolution was 2–3 mm with an acquisition time of 160–235 msec per slice. The sequence was set to the following: repetition time 2.5 msec per phase encoding step, echo time 1.2 msec, flip angle $\alpha = 18$ degrees, matrix size 60–90 \times 128 (phase encoding \times readout points), a rectangular field of view of 280–330 mm, a slice thickness of 10 mm, and an interslice gap of 3–5 mm.

Studies were obtained during an antecubital bolus injection of 4–7 ml gadolinium-DTPA (0.03 mmol/kg body weight). The preloaded contrast bolus was flushed through the intravenous line with 15 ml normal saline at a rate of 10 ml/sec using a power injector (Medrad, Pittsburgh, PA). Image acquisition was electrocardiogram (ECG)-gated, and acquisition started 10 msec after the end of a nonselective saturation-recovery magnetization preparation that was triggered by the detection of an R wave. Image acquisition was started 3–4 heartbeats before injection of the contrast material, and 40 images per slice were obtained to follow the contrast bolus through the circulation. ECG gating allowed acquisition of images at a fixed time point in the cardiac cycle, and the myocardial wall motion appeared frozen.

Fourteen rest and 3 hyperemic first-pass perfusion studies acquired in the left ventricular (LV) short axis were included in the analysis. Hyperemia was induced as part of the study protocol in three patients (one patient with microvascular dysfunction, one with cardiomyopathy, and one with previous bypass surgery) by increasing doses (70–100–140 $\mu\text{g}/\text{kg}/\text{min}$) of intravenous adenosine over a period of 4 min and constant monitoring with consecutive image acquisition. Indication for hyperemic imaging was the detection of regional or global ischemia.

Assessment of Image Quality

The quality of each study was graded individually as excellent, good, or poor by consensus of each of the two observers according to the criteria outlined in Table 2. The observers considered the dispersion of the contrast bolus in the left ventricle, the endo-/epicardial border delineation, trigger artifacts, and patient stature (body mass index) and cooperation. A body mass index > 30 was rated as 0. A contrast bolus was rated as 0 if the time interval between half-maximal contrast enhancement in the left ventricle from the up to the down slope of the signal intensity curve was more than 16 heartbeats. Trigger artifacts were rated as 0 if different phases of the

Table 2
Criteria and Scheme for the Evaluation of Image Quality

Parameter	Yes	No	Image Quality
Dispersed contrast bolus in left ventricle	0	1	Excellent, 4
Restricted endo-/epicardial border delineation	0	1	
Trigger artifacts	0	1	Good, 2–3
Patient parameters (increased BMI)	0	1	Poor, 0–1

BMI, body mass index.

cardiac cycle were acquired during scanning. In this case, the myocardial contours had different circumferences in consecutive image frames. This complicated the automated segmentation algorithm and therefore required additional user intervention for an optimal contour-border match. An example of a study with good and a study with poor quality are shown in Fig. 1.

Image Analysis

The studies were archived to an optical disk and transferred to a SPARC 10 Workstation (Sun Microsystems, Mountain View, CA). For analysis, a mid-LV slice was selected from each patient study.

The studies were analyzed and regional transmural signal/time intensity curves were obtained using the Argus Cardiac Image Analysis software (Siemens, Iselin, NJ). The two observers were blinded to the results obtained by the other observer and analyzed the studies by following a set protocol. For interobserver agreement, observer 1 and 2 analyzed 17 studies. For intraobserver agreement, observers 1 and 2 each analyzed the first 10 of the 17 studies a second time. The second analysis was done 1 week after the initial analysis.

As the initial step of the data analysis, the user selected the image with the brightest contrast between the LV cavity and the myocardium (Fig. 2, step 1) as a reference image. The observer then drew endocardial and epicardial contours on this image (Fig. 2, step 2). The automatic segmentation algorithm matched the contours of the endocardial and epicardial borders to all remaining images of the study so that the contours in each frame were at the same position as in the reference image. Usually, only a few manual corrections had to be applied to

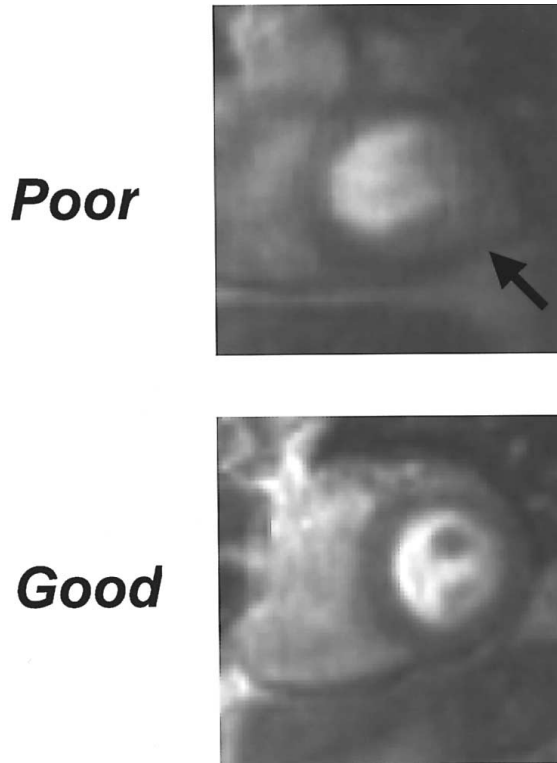


Figure 1. Images with poor (top) and good (bottom) quality. Both images show the maximal contrast enhancement of the left ventricle in the individual study. The upper image shows only weak contrast enhancement with consecutively reduced endocardial border delineation. Furthermore, signal inhomogeneities with reduced signal in the posterolateral wall are seen (black arrow).

the automatic positioning of the endocardial and epicardial contours for satisfactory matching.

The LV myocardial ring was then divided into eight sectors of equal size. In seven of the 17 studies, 9 regions were analyzed with three anterior regions instead of two. To allow for anatomic matching from repeated analysis of the same study, the reference sector was defined at the anterior junction of the epicardium of the left and right ventricle in every study (Fig. 2, step 3). Spatially averaged image intensity values were used to calculate signal intensity versus time data.

Assessment of Signal-to-Noise Ratio

The signal-to-noise ratios were determined once in every study by one observer. The observer then drew regions of interest in the anteroseptal (signal), the posterolateral region (signal), and a region outside the body

(noise) in three precontrast images. Signal and noise were measured once in each of the precontrast images. The resulting three values were averaged.

Contrast Dosage

A low dosage (0.03 mmol/kg) Gd-DTPA for quantitative perfusion studies was used. This was because MR contrast agents such as Gd-DTPA show a linear relation between contrast concentration and progression of signal intensity only in a dose range of 0.2 to 2.0 mmol/l (6,7).

Perfusion Modeling

Model-constrained deconvolution was used to calculate the maximum amplitude of the impulse response (R_{\max}) and the maximum change of signal intensity (ΔSI_{\max}) of the contrast bolus (8):

$$m(t) = c_{\text{in}}(t) \times R(t)$$

where $m(t)$ is the mass of the contrast material detected by MR and $c_{\text{in}}(t)$ is the input function represented by the tissue signal curve in the left ventricle. The input function is mandatory for the quantitative analysis of the tissue signal curves because of varying hemodynamic conditions and the characteristics of the contrast bolus. $R(t)$ is constrained to the shape of a Fermi function, which provides an appropriate parameterized measure of the tissue impulse response function (9) (Figs. 3 and 4); $R(t)$ can be used as a measure of flow.

Statistical Analysis

Intra- and interobserver agreements were determined with the intraclass correlation coefficient (R) by using repeated measurement analysis of variance (ANOVA) (10,11).

$$R = \frac{\sigma_{\text{sub}}^2}{\sigma_{\text{sub}}^2 + \sigma_{\text{obs}}^2 + \sigma_{\text{err}}^2}$$

where σ_{sub}^2 is the within-subject variation, σ_{obs}^2 is the variance between observations, and σ_{err}^2 is error variance (typical error).

R is expressed as a number between 0 and 1. A value between 0.7 and 0.9 was defined as a good agreement between observations. The interpretation of R is further facilitated by reporting the precision of the subjective scoring represented by the standard error of the measurement (s.e.m.) defined in terms of SD of R_{\max} and ΔSI_{\max} :

$$\text{s.e.m.} = \text{SD} \times (1 - R)^{1/2}$$

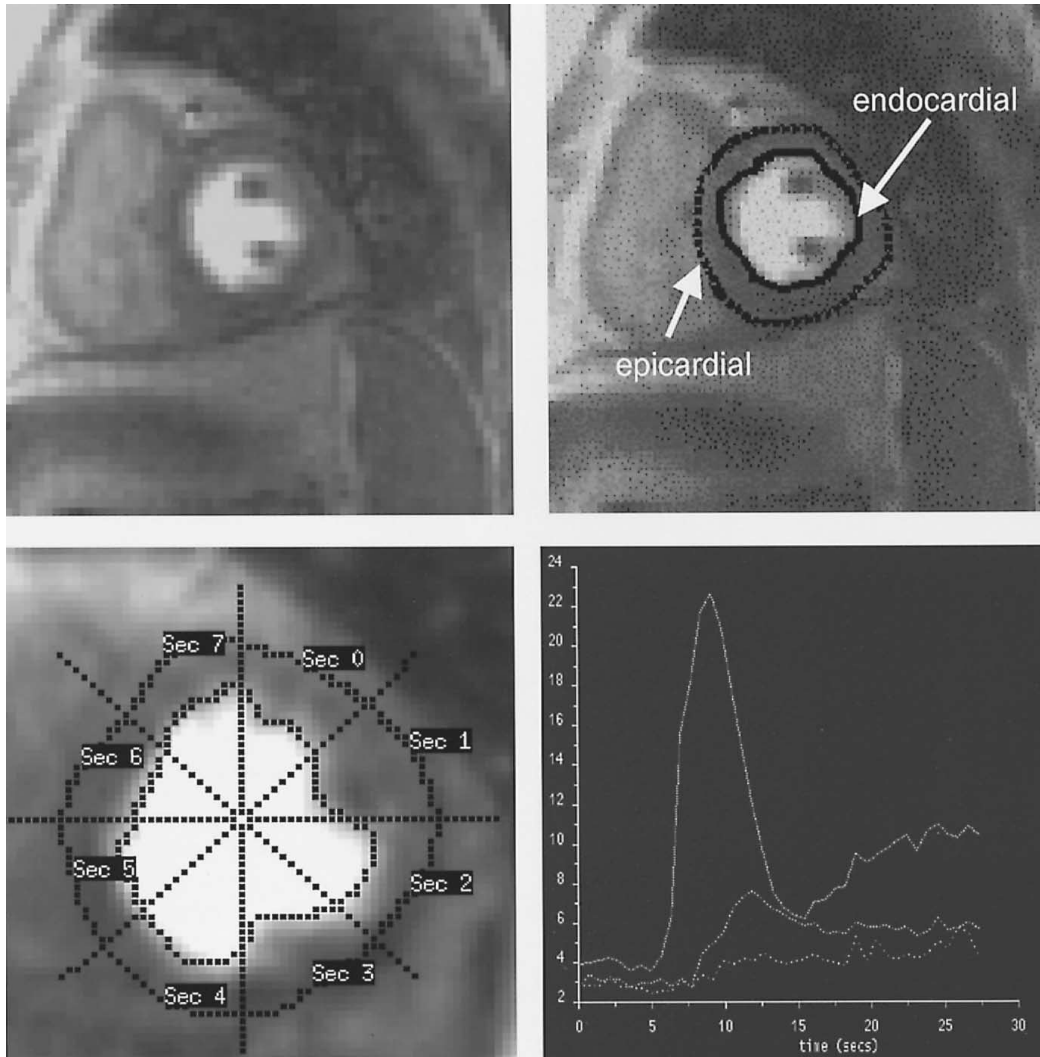


Figure 2. Perfusion analysis with dedicated cardiac software. (Top left) The image with the brightest contrast enhancement in the LV cavity of the individual study was chosen (step 1) and (top right) endocardial (arrow) and epicardial (arrow) borders were drawn in this image (step 2). An automated edge detection algorithm applied the segmentation to the remainder of the image frames (not shown). (Bottom left) Eight sectors were chosen with the reference sector at the right-left ventricle border (step 3). (Bottom right) The program then calculates the signal/time-intensity values (step 4) (raw values before applying the fitting algorithm are plotted).

Precision of measurements was further defined by the 95% confidence interval (CI). The relationship between sample size (N) and the CI is

$$N = (Z_{\alpha/2}/CI)^2 + 3$$

where $Z = 1.96$ for 95% CI. R was determined for the entire ring and for the separate myocardial regions before and after exclusion of studies with poor quality.

Bland-Altman analysis (12) was performed for inter-observer R_{\max} and ΔSI_{\max} to graphically depict agreement

between two measurements. Variability was given as the mean of difference of the individual data pair per mean of the individual data pair.

For comparison of two sets of measurements by one observer or between the measurements by two observers and the signal-to-noise ratio of the regions within one patient (anteroseptal vs. posterolateral), a paired t -test was used. To compare data (\pm SE) between two groups of patients, a t -test for unpaired data was used. A $p < 0.05$ was considered to be statistically significant.

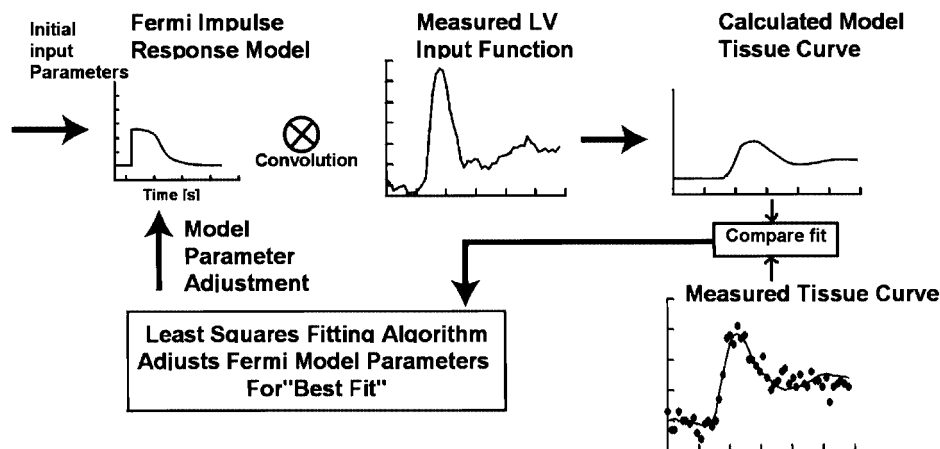


Figure 3. Flow chart of the steps involved to create the signal residue curves using the Fermi function model and constrained deconvolution. First, convolution of the measured LV input function with the Fermi impulse response model creates an estimated model tissue curve. Second, the estimated model tissue curve is compared with the measured tissue curve. The fitting algorithm then adjusts the model parameters to minimize the differences between the estimated and the true curves to create the impulse response function.

RESULTS

Image acquisition was successfully performed in all patients. All patients tolerated the imaging procedure and contrast and adenosine administration well. Total study time per patient was approximately 35–45 min, including the acquisition of the hyperemic images in three patients. During adenosine infusion, some patients experienced shortness of breath ($n = 2$) or chest discomfort ($n = 2$). The study quality was graded as poor in three studies

(18%), good in eight studies (47%), and excellent in six studies (35%) by agreement of the two observers. Poor quality was accounted for by a dispersed contrast bolus in two patients (mean bolus time 21 ± 4 heartbeats vs. 12 ± 2 in the remaining 12 patients; $p < 0.01$) and suboptimal ECG trigger signal due to coughing during image acquisition and/or increased body mass index in three patients (mean body mass index 36.8 ± 3.7 , $n = 3$). A total of 136 regions was analyzed for interobserver agreement. The signal residue curves of two regions (1.4%)

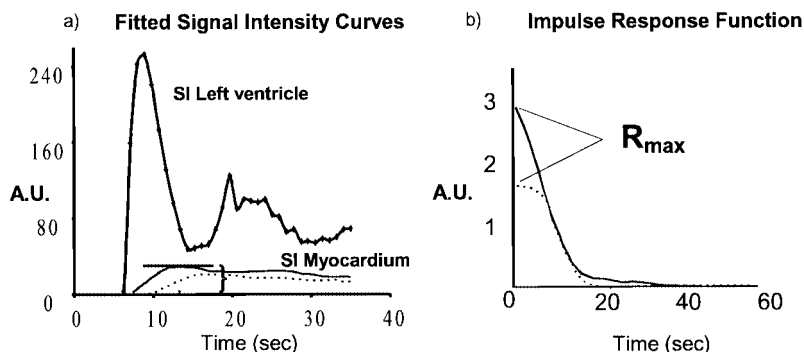


Figure 4. (a) The graph shows the LV signal-/time-intensity curve, which serves as the input function, and tissue signal-/time-intensity curves (after fitting the raw values) of two different myocardial regions (solid and dashed). The change in signal intensity (ΔSI_{max}) was determined based on the fitted curves. (b) Based on the area over height principle, the maximum amplitude of the tissue impulse response function (R_{max}) is calculated. The impulse response function in red (blue) corresponds to the red (blue) myocardial signal intensity curve of a. The higher amplitude of the red compared with the blue curve indicates a higher perfusion in the region represented by the red curve. A.U., arbitrary units.

were excluded due to artifacts induced in the fitting algorithm. For intraobserver agreement, 10 studies (two poor [20%], five good [50%], three excellent [30%] image quality, two hyperemia studies) were quantified by each of the two observers with a total of 2×80 regions. None of these regions had to be excluded. The mean time required for the analysis of one slice was 25 ± 8 min (range, 20–40 min).

Signal-to-Noise Ratio

Overall, signal-to-noise ratios in the anteroseptal myocardium were significantly higher versus the posterolateral regions (3.7 ± 1.5 vs. 2.9 ± 1.0 , $p < 0.01$). The signal-to-noise ratios observed in the posterolateral region of the studies with excellent to good quality were significantly higher versus studies with poor quality (3.0 ± 0.6 vs. 2.2 ± 0.3 , $p < 0.05$).

Intraobserver Agreement

For intraobserver agreement, the means of R_{max} and ΔSI_{max} were not significantly different (R_{max} : 1.68 ± 0.10 and 1.61 ± 0.09 , $p = 0.12$; ΔSI_{max} : 22.2 ± 0.6 and 22.7 ± 0.6 , $p = 0.08$, $n = 160$). The intraobserver agreement for R_{max} and ΔSI_{max} were good with $R = 0.85$ and 0.80 (95% CI, 0.72–2.58 and 16.1–28.8, $n = 160$; variability, $23 \pm 2\%$ and $11 \pm 1\%$). After exclusion of the studies with poor quality, the means for R_{max} and ΔSI_{max} were not significantly different (1.36 ± 0.07 vs. 1.35 ± 0.07 , $p = 0.84$, 22.5 ± 0.6 vs. 22.4 ± 0.6 , $p = 0.64$, $n = 112$). The intraobserver agreement for R_{max} and ΔSI_{max} increased from good to excellent (0.85 to 0.93 and 0.80 to 0.93), whereas the 95% CI decreased (0.96–1.74 and 18.9–25.9, $n = 112$; variability, $21 \pm 2\%$ and $11 \pm 1\%$), indicating higher precision.

Interobserver Agreement

The means of R_{max} for observer 1 (1.40 ± 0.07) and observer 2 (1.52 ± 0.08) were significantly different ($p < 0.02$, $n = 134$). After exclusion of the studies with poor quality, the means were no longer significantly different (1.32 ± 0.07 vs. 1.38 ± 0.08 , $p = 0.27$, $n = 110$). The means of ΔSI_{max} were 21.1 ± 0.6 and 21.8 ± 0.7 ($p < 0.05$) for observers 1 and 2. After exclusion of studies, with poor image quality, ΔSI_{max} was 21.1 ± 0.7 for observer 1 and 21.7 ± 0.7 for observer 2 ($p < 0.07$).

The overall interobserver agreement of R_{max} was only fair with $R = 0.55$ (95% CI, 0.30–2.58; $n = 134$; variability, $23 \pm 2\%$). Interobserver agreement and improved

Table 3

Interobserver Agreement of the Maximum Amplitude of the Impulse Response Function Before and After Exclusion of Studies with Poor Quality

Region	Total (n = 34)		Good and Excellent Image Quality (n = 28)	
	R	95% CI	R	95% CI
Anterior	0.81	1.0–2.0	0.94	1.0–1.8
Lateral	0.69	0.4–1.9	0.97	0.8–1.3
Posterior	0.65	0.5–2.3	0.94	0.9–1.7
Septal	0.82	1.0–2.8	0.81	0.8–2.5

R_{max} , maximum amplitude of the impulse response function; R, interobserver agreement; 95% CI, 95% confidence interval.

remarkably when studies with poor quality was excluded ($R = 0.88$), together with an increasing precision (95% CI, 0.84–1.92; $n = 112$; variability, $21 \pm 1\%$). ΔSI_{max} showed a better interobserver agreement with $R = 0.73$ (95% CI, 13.4–29.6; $n = 134$; variability, $14 \pm 1\%$) and improved slightly to 0.83 (95% CI, 14.9–27.8; $n = 117$; variability, $13 \pm 1\%$) when study quality was considered. The R values and 95% CI for the individual myocardial regions are shown in Tables 3 and 4.

The Bland-Altman analysis for R_{max} and ΔSI_{max} are shown in Figs. 5 and 6. There is an increasing scatter toward higher numbers of R_{max} , whereas ΔSI_{max} shows a more homogenous scatter over the range of data. For R_{max} the variability was 23% and R_{max} values and variability were positively correlated ($r = 0.60$, $p < 0.01$), indicating higher variability with higher R_{max} values. The vari-

Table 4

Interobserver Agreement of the Change in Signal Intensity of the Contrast Bolus Before and After Exclusion of Studies with Poor Quality

Region	Total (n = 34)		Good and Excellent Image Quality (n = 28)	
	R	95% CI	R	95% CI
Anterior	0.77	13.8–28.4	0.77	13.6–29.9
Lateral	0.91	13.5–20.3	0.90	12.0–20.3
Posterior	0.81	15.2–26.9	0.93	17.0–24.0
Septal	0.81	20.5–33.0	0.77	19.8–32.5

ΔSI_{max} , change in signal intensity; R, interobserver agreement; 95% CI, 95% confidence interval.

Copyright © Marcel Dekker, Inc. All rights reserved.

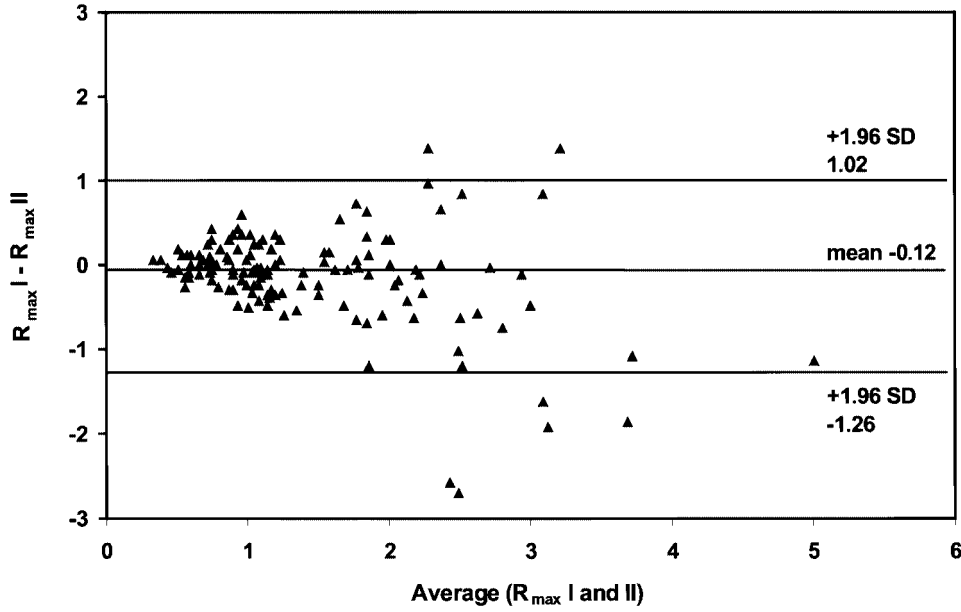


Figure 5. Bland-Altman plot of the values calculated for the maximum change of the impulse response function derived from the analysis of observer 1 (R_{\max} I) and observer 2 (R_{\max} II).

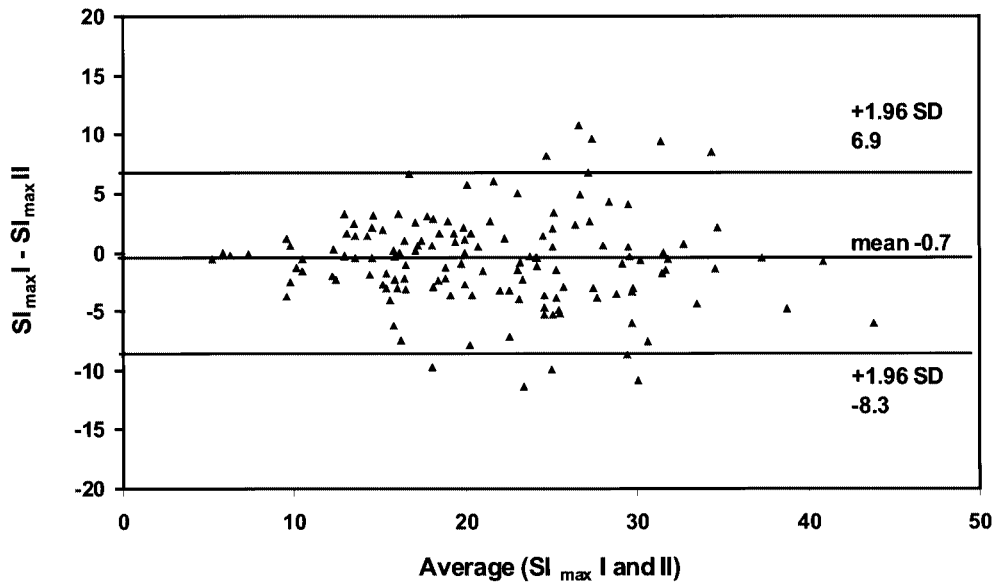


Figure 6. Bland-Altman plot of the values calculated for the change in signal intensity derived from the analysis of observer 1 (ΔSI_{\max} I) and observer 2 (ΔSI_{\max} II).

ability of ΔSI_{\max} was 13%. The correlation of ΔSI_{\max} values and variability was not as strong ($r = 0.29$, $p < 0.01$) compared with R_{\max} .

DISCUSSION

Perfusion analysis with quantitative MRFP imaging provides a new noninvasive technique to quantify myocardial blood flow in patients with coronary artery disease, microvascular dysfunction, myocardial infarction, or heart failure (1,4,13). MR has been used to follow up collateral flow (14) and angiogenesis (3) in animal studies after treatment with newly developed revascularization methods.

The current study demonstrates that MRFP imaging is a method with good intraobserver ($R = 0.80$ – 0.85) agreement. The interobserver agreement of the quantitative perfusion analysis is highly dependent on image quality. The R value and precision of the measurement for R_{\max} increased remarkably from 0.55 to 0.88 when studies with poor quality were excluded. When myocardial regions were analyzed individually, the interobserver agreement for R_{\max} was 0.81, 0.69, 0.65, and 0.82 for the anterior, lateral, posterior, and septal regions, respectively, and increased to 0.94, 0.97, 0.94, and 0.81, respectively, in studies with good or excellent quality compared with all studies. The individual analysis of the myocardial regions showed that the agreement was predominantly restricted in the posterior and lateral regions. Those regions have a lower signal-to-noise ratio and are more prone to image artifacts, whereas the anterior wall and the septum were affected to a lesser degree. This reflects the drop-off in sensitivity as a function of distance from the surface coil elements, which results in a poorer signal-to-noise ratio in the posterior segments compared with the anterior segments. Bottomley et al. (15) showed that the signal-to-noise ratio before contrast in the posterolateral regions of the heart have an average value of 1.47–2.37, whereas the anteroseptal regions have an average value of 1.98–4.37 relative to a body coil. The relationship of their values was in good agreement with results of our study (anteroseptal, 2.02–5.78; posterolateral, 1.71–4.49).

Several authors demonstrated that optimized coils could markedly improve the signal-to-noise ratio in cardiac imaging (15–17). In addition, an increased acquisition frequency (i.e., higher temporal resolution) and pulse sequences with higher signal yield, such as a true fast imaging by steady precession sequence in combination

with newly designed cardiac surface coils, will improve the achievable signal-to-noise ratio.

The degree to which a reduced signal-to-noise or contrast-to-noise ratio impairs the quantitative analysis depends also on the analysis algorithm. Semiquantitative parameters derived from signal intensity time curves such as the change in signal intensity (our ΔSI_{\max}) are less sensitive to study quality and noise than the maximum amplitude of the impulse response function (R_{\max}), a parameter deriving from deconvolution of the tissue curves.

The intra- and interobserver agreements of MRFP imaging are in good accordance with data derived from methods that are already routinely used for myocardial perfusion imaging. The R scores of planar thallium-201 scintigraphy (18) ranged from 0.72 to 0.91 for all regions and from 0.54 to 0.92 for individual segments.

Sawada et al. (19) assessed interobserver reproducibility with positron emission tomography and reported a higher r value (0.96) compared with our method of MRFP perfusion imaging. However, this study shows two main differences compared with our present study. First, a correlation coefficient (r) instead of an *intraclass* correlation coefficient obtained by repeated measurement ANOVA was used in that study (19), and Brambilla et al. (18) outlined the advantages of *intraclass* correlation coefficient to determine agreement between two measurements. Compared with the determination of inter- or intraobserver variance or correlation coefficient (r), the *intraclass* correlation coefficient based on ANOVA takes chance agreement, partial disagreement, and systematic differences into account. A limitation of the inter- or intraobserver *variance* as a measure of R is that it neglects the variance between subjects (σ_{sub}^2). The correlation coefficient (r) does not account for systematic differences between observers (σ_{obs}^2).

Second, half of the subjects in the positron emission tomography study (19) were normal control subjects. The study quality will be better in a normal population compared with patients with coronary artery disease. We assume that in patients as seen in our study, the contrast-to-noise ratio may have been reduced by typical patient characteristics such as obesity or sternal wires.

CONCLUSION AND CLINICAL IMPLICATION

For good image quality, MRFP imaging showed a good intraobserver and interobserver agreement. Individual regions showed a good to excellent interobserver



agreement, which implies reliable evaluation of MRFP imaging in patients with individual vessel lesions. Our results encourage employment of quantitative MRFP imaging in longitudinal clinical trials to follow-up myocardial perfusion changes. Perfusion studies assessing interstudy reproducibility of this method are underway.

Because MRFP imaging allows reliable analysis of myocardial blood flow and accounting for the higher costs and lower accessibility to positron emission tomography centers, cardiac MR imaging might be more advantageous in respect to multicenter clinical perfusion trials.

ACKNOWLEDGMENT

Olaf Mühling was supported by a grant from the "Deutsche Forschungsgemeinschaft" (MU 1570/1-1) as a postdoctoral research associate in cardiac imaging. We acknowledge Michael J. Kleindl, RT (RMR) for continuous support in data acquisition, patient care, and management.

REFERENCES

1. Wilke, N.; Jerosch-Herold, M.; Wang, Y.; Huang, Y.; Christensen, B.V.; Stillman, A.E.; Ugurbil, K.; McDonald, K.; Wilson, R.F. Myocardial Perfusion Reserve: Assessment With Multisection, Quantitative, First-Pass MR Imaging. *Radiology* **1997**, *204*, 373-384.
2. Jerosch-Herold, M.; Huang, Y.; Huang, H.; Wilke, N.; Zenovich, A.; Zhao, F.; Gurchumelidze, S. MRI Assessment of Collateral Development in Porcine Model of Chronic Ischemia. *J. Cardiovasc. Magn. Reson.* **1999**, *1*, 269 [Abstract].
3. Pearlman, J.D.; Laham, R.J.; Simons, M. Coronary Angiogenesis: Detection In Vivo With MR Imaging Sensitive to Collateral Neocirculation—Preliminary Study in Pigs. *Radiology* **2000**, *214*, 801-807.
4. Jerosch-Herold, M.; Wilke, N. MR First Pass Imaging: Quantitative Assessment of Transmural Perfusion and Collateral Flow. *Int. J. Cardiol. Imaging* **1997**, *13*, 205-218.
5. Kroll, K.; Wilke, N.; Jerosch-Herold, M.; Wang, Y.; Zhang, Y.; Bache, R.J.; Bassingthwaighe, J.B. Modeling Regional Myocardial Flows From Residue Functions of an Intravascular Indicator. *Am. J. Physiol.* **1996**, *271*, H1643-H1655.
6. Koenig, S.H.; Spiller, M.; Brown, R.D., III.; Wolf, G.L. Relaxation of Water Protons in the Intra- and Extracellular Regions of Blood Containing Gd (DTPA). *Magn. Reson. Med.* **1986**, *3*, 791-795.
7. Strich, G.; Hagan, P.L.; Gerber, K.H.; Slutsky, R.A. Tissue Distribution and Magnetic Resonance Spin Lattice Relaxation Effects of Gadolinium-DTPA. *Radiology* **1985**, *154*, 723-726.
8. Jerosch-Herold, M.; Wilke, N.; Stillman, A.E. Magnetic Resonance Quantification of the Myocardial Perfusion Reserve With a Fermi Function Model for Constrained Deconvolution. *Med. Phys.* **1998**, *25*, 73-84.
9. Axel, L. Tissue Mean Transit Time From Dynamic Computed Tomography by a Simple Deconvolution Technique. *Invest. Radiol.* **1983**, *18*, 94-99.
10. Streiner, D.L.; Norman, G.R. *Health Measurement Scales*. Oxford University Press: New York, 1991, 79-95.
11. Wiener, B.J. *Statistical Principles in Experimental Design*. McGraw Hill: New York, 1971, 283-285.
12. Bland, J.M.; Altman, D.G. Statistical Methods for Assessing Agreement Between Two Methods of Clinical Measurement. *Lancet* **1986**, *1*, 307-310.
13. Wilke, N.; Jerosch-Herold, M. Assessing Myocardial Perfusion in Coronary Artery Disease With Magnetic Resonance First-Pass Imaging. *Cardiol. Clin.* **1998**, *16*, 227-246.
14. Jerosch-Herold, M.; Wilke, N.; Rodenwaldt, J.; Mansoor, A.; Gurchumelidze, S.P.; Zenovich, A. MRI Measurements of Perfusion Reserve in Collateral-Dependent Myocardium of Pigs. *Circulation* **1999**, *100*, I-225 [Abstract].
15. Bottomley, P.A.; Lugo Olivieri, C.H.; Giaquinto, R. What Is the Optimum Phased Array Coil Design for Cardiac and Torso Magnetic Resonance? *Magn. Reson. Med.* **1997**, *37*, 591-599.
16. Constantinides, C.D.; Westgate, C.R.; O'Dell, W.G.; Zehouni, E.A.; McVeigh, E.R. A Phased Array Coil for Human Cardiac Imaging. *Magn. Reson. Med.* **1995**, *34*, 92-98.
17. Fayad, Z.A.; Connick, T.J.; Axel, L. An Improved Quadrature or Phased-Array Coil for MR Cardiac Imaging. *Magn. Reson. Med.* **1995**, *34*, 186-193.
18. Brambilla, M.; Inglese, E.; Cannizzaro, G.; Dondi, M.; Sara, R.; Arrigo, F.; Tarolo, G.L. A Multicenter Trial on Interobserver and Intraobserver Reproducibility of Segmental Scoring of Thallium-201 Planar Myocardial Imaging Before and After Reinjection. *Italian Group of Nuclear Cardiology. J. Nucl. Med.* **1994**, *35*, 601-608.
19. Sawada, S.; Muzik, O.; Beanlands, R.S.B.; Wolfe, E.; Hutchins, G.D.; Schwaiger, M. Interobserver and Interstudy Variability of Myocardial Blood Flow and Flow-Reserve Measurements With Nitrogen 13 Ammonia-Labeled Positron Emission Tomography. *J. Nucl. Cardiol.* **1995**, *2*, 413-422.



Request Permission or Order Reprints Instantly!

Interested in copying and sharing this article? In most cases, U.S. Copyright Law requires that you get permission from the article's rightsholder before using copyrighted content.

All information and materials found in this article, including but not limited to text, trademarks, patents, logos, graphics and images (the "Materials"), are the copyrighted works and other forms of intellectual property of Marcel Dekker, Inc., or its licensors. All rights not expressly granted are reserved.

Get permission to lawfully reproduce and distribute the Materials or order reprints quickly and painlessly. Simply click on the "Request Permission/Reprints Here" link below and follow the instructions. Visit the [U.S. Copyright Office](#) for information on Fair Use limitations of U.S. copyright law. Please refer to The Association of American Publishers' (AAP) website for guidelines on [Fair Use in the Classroom](#).

The Materials are for your personal use only and cannot be reformatted, reposted, resold or distributed by electronic means or otherwise without permission from Marcel Dekker, Inc. Marcel Dekker, Inc. grants you the limited right to display the Materials only on your personal computer or personal wireless device, and to copy and download single copies of such Materials provided that any copyright, trademark or other notice appearing on such Materials is also retained by, displayed, copied or downloaded as part of the Materials and is not removed or obscured, and provided you do not edit, modify, alter or enhance the Materials. Please refer to our [Website User Agreement](#) for more details.

[Order now!](#)

Reprints of this article can also be ordered at

<http://www.dekker.com/servlet/product/DOI/101081JCMR100107473>